Behavioral/Systems/Cognitive

Ongoing Temporal Coding of a Stochastic Stimulus as a Function of Intensity: Time-Intensity Trading

Pascal Michelet, Damir Kovačić, and Philip X. Joris
Laboratory of Auditory Neurophysiology, Medical School, Campus Gasthuisberg, University of Leuven, B-3000 Leuven, Belgium

Stimulus-locked temporal codes are increasingly seen as relevant to perception. The timing of action potentials typically varies with stimulus intensity, and the invariance of temporal representations with intensity is therefore an issue. We examine the timing of action potentials in cat auditory nerve to broadband noise presented at different intensities, using an analysis inspired by coincidence detection and by the binaural "latency hypothesis." It is known that the two cues for azimuthal sound localization, interaural intensity or level differences and interaural time differences (ITDs), interact perceptually. According to the latency hypothesis, the increase in intensity for the ear nearest to a sound source off the midline causes a decrease in response latency in that ear relative to the other ear. We found that changes in intensity cause small but systematic shifts in the ongoing timing of responses in the auditory nerve, generally but not always resulting in shorter delays between stimulus onset and neural response for increasing intensity. The size of the temporal shifts depends on characteristic frequency with a pattern indicating a fine-structure and an envelope response regime. Overall, the results show that ongoing timing is remarkably stable with intensity at the most peripheral neural level. The results are not consistent in a simple way with the latency hypothesis, but because of the acute sensitivity to ITDs, the subtle effects of intensity on timing may nevertheless have perceptual consequences.

Introduction

Temporal features of neuronal responses attract increasing interest as candidate neural codes (Rieke et al., 1997). A simple temporal code is response latency, i.e., the timing of spikes relative to stimulus features such as its onset (Brugge et al., 1996; Furukawa et al., 2000; Johansson and Birznieks, 2004; VanRullen et al., 2005; Sawtell et al., 2006; Chase and Young, 2007; Gollisch and Meister, 2008; Shusterman et al., 2011; Zohar et al., 2011). Because increasing stimulus intensity generally causes a decrease in response latency (Adrian, 1928), intensity is a potential confound.

An interesting test case is in hearing, where temporal stimulus coding is essential to detect tiny interaural time differences (ITDs), which are a cue to azimuthal sound location. The question arises how this system copes with changes in intensity. If the intensities at the two ears would always be equal, changes in latency due to changes in sound intensity would be irrelevant because the spike timing of one auditory nerve (AN) relative to the other would not be affected. However, a sound off the midline reaches the two ears not only at different times but also with different intensity. Such interaural intensity or level differences (ILDs) could potentially cause opposite latency changes in left and right AN. This could be detrimental because it complicates the relationship between ITD and spatial location, or could be beneficial because ILD and ITD covary (Gaik, 1993) so that ILD could actually magnify the effective temporal differences conveyed to binaural neurons.

Behavioral studies show that ILD is a cue to azimuthal position in itself, and that the two cues (ITD and ILD) can be traded against each other. In "time-intensity trading" experiments, localization is toward the right ear if an ITD favors that ear, and is brought toward the other side by increasing the intensity at the left ear (Durlach and Colburn, 1978). A simple substrate for such observations would be an interaction at the single neuron level.

The "latency hypothesis" places ILD–ITD interaction at the most peripheral neural level: the AN (Jeffress, 1948). The basic idea is that ILD is transformed into an "internal" delay by latency shifts in the monaural pathways. Thus, an ILD favoring the right ear would cause localization toward that side by virtue of a time difference, created in the brain through latency shifts, which favors the same ear. A simple cue conversion as proposed by the latency hypothesis is contradicted by psychophysical studies but is to some extent supported by physiological studies (Hirsch et al., 1985; Pollak, 1988; Heil, 1998; Irvine et al., 2001). However, the latter studies focused on transient responses. It is well known that spike timing of the onset and sustained part of the response behave differently e.g., to the intensity of pure tones (Moller, 1975; Joris and Smith, 1998; Chase and Young, 2007). Moreover, ongoing timing cues rather than onset timing underlie the exquisite behavioral sensitivity to ITDs (Buell et al., 1991). It is there-

Received Jan. 8, 2012; revised May 13, 2012; accepted May 18, 2012.

Author contributions: P.X.J. designed research; P.M., D.K., and P.X.J. performed research; P.M., D.K., and P.X.J. analyzed data; P.M. and P.X.J. wrote the paper.

This work was supported by the Fund for Scientific Research–Flanders (G.0392.05 and G.0633.07), and Research Fund University of Leuven (OT/05/57 and OT/09/50). P.M. was supported by IWT (Agentschap voor Innovatie door Wetenschap en Technologie); D.K. was supported by a Marie-Curie fellowship (GA 221755). The technical help of P. Kayenbergh and G. Meulemans is kindly acknowledged.

The authors declare no competing financial interests.

Correspondence should be addressed to Philip X. Joris, Laboratory of Auditory Neurophysiology, Campus Gasthuisberg O/N2, K.U. Leuven, Herestraat 49 bus 1021, B-3000 Leuven, Belgium. E-mail: Philip.Joris@med.kuleuven.be.

DOI:10.1523/JNEUROSCI.0103-12.2012

 0270-6474/12/329517-11$15.00/0

fore important to examine how ongoing spike timing is affected by intensity.

Materials and Methods

We examine the effects of stimulus level of a sustained broadband noise on the temporal coding in the AN with a coincidence analysis. A preliminary report was published earlier (Joris et al., 2008b). We recorded spike-trains from the AN of eight cats, of either sex, with clear eardrums. All procedures were approved by the K.U. Leuven Ethics Committee for Animal Experiments. Recordings were made in a soundproof room (Industrial Acoustics). Induction of anesthesia was with an i.m. injection of a 1:3 mixture of Acepromazine and Ketamine. During surgery and recording, anesthesia was monitored with nociceptive reflexes, and supplementing i.v. injections of pentobarbital were given when deemed necessary. The animal's body temperature was monitored with a rectal probe, and was kept at 37°C by means of a heating blanket. Following a tracheotomy, the outer ear and temporalis muscle were removed unilaterally. The bulla was vented using a 30 cm polyethylene tube (0.9 mm inner diameter) to prevent static pressure build-up. Some portions of the cerebellum were aspirated through a fossa posterior craniotomy to visualize the AN. Glass microelectrodes filled with 3 M NaCl (impedance typically 40–60 MΩ) were then advanced into the AN using a hydraulic microdrive attached to a chamber placed over the craniotomy. Warm agar (3%) was used to seal the craniotomy.

Stimuli and neural recording. A dynamic speaker attached to a plastic earpiece was inserted into the transected ear canal. The acoustic transfer function of this assembly was measured with a probe and microphone (Bruel and Kjaer) close to the eardrum, and was compensated for in the stimuli. The neural signal was buffered, filtered (300–3000 Hz; DAM 80, World Precision Instruments), amplified, visualized and audio-monitored in conventional ways. Action potentials were timed with a peak-detecting circuit. Standard timing pulses from the peak-detector were time stamped with 1 μs precision (TDT ET1, Tucker-Davis Technologies).

While advancing the electrode, we searched for auditory driven spikes by using tone pips ascending in frequency. Only well isolated single fibers were studied. We first obtained a threshold curve with a tracking algorithm, which estimated characteristic frequency (CF, frequency of lowest threshold) and spontaneous rate (SR, measured over a 15 s silent interval). Gaussian pseudorandom broadband (50–32,000 Hz) noise 1000 ms in duration was then presented. Within an experiment, a single noise token was typically used. For reasons that have been stated in earlier reports and which will be repeated in Results, we delivered the noise in "standard" and "inverted" polarity (as if inverting the leads to the speaker), henceforth referred to as the A+ and A− stimuli, in two blocks of usually 50 repetitions (random order) for each polarity. The repetition interval was 1200 ms (interstimulus interval of 200 ms).

The main stimulus variable of interest was sound pressure level (expressed in dB SPL, i.e., referenced to 20 μPa), which was varied in steps of 10 dB or sometimes 5 dB if time allowed. For each fiber, we tried to obtain responses to as many stimulus levels as possible. The sequence of SPLs was arbitrary but not entirely random. Since holding times of AN fibers are limited and we wished to have datasets for similar SPLs for as many fibers as possible (see Results; Fig. 4), we first collected data at a number of "favored" SPLs, e.g., 70, 90, 50 dB, and then obtained responses to additional levels to the extent possible.

Coincidence analysis and general approach. To analyze the effects of stimulus level on ongoing timing in the AN, we performed a coincidence analysis, as described in previous publications (Joris, 2003; Louage et al., 2004; Joris et al., 2006b). In that earlier work coincidences were computed across spike-trains obtained from a single fiber to a single stimulus (e.g., a single noise token at a single SPL), or sometimes across spike-trains from different fibers to a single stimulus (Joris et al., 2006a). Here, we will compute coincidences across spike-trains, again from responses of a single fiber to a single waveform, but obtained at different SPLs. The procedure is illustrated in Figure 1 with two sets of fictional spike-trains at "test" SPL_X and "reference" SPL_{ref}. The latter was taken at 70 dB except where noted. This choice is arbitrary, but the pattern of results does not depend on the choice of SPL_{ref}. We select a spike in one of the spike-trains at SPL_X, and calculate the intervals between this spike and all the spikes in the responses at SPL_{ref}. The correlogram is a histogram of all measured intervals: each interval is represented as an entry into the corresponding bin. Positive intervals indicate a lag of the response at SPL_{ref} (relative to SPL_X) and are labeled as positive delays in the figures. Negative intervals indicate a lead of the response at SPL_{ref} and are labeled as negative delays in the figures. Because the window used to determine whether two spikes are coincident is 50 μs (a choice based on previous coincidence analyses, Joris et al., 2006a), each bin in the histogram in Figure 1 is 50 μs wide. Once all the intervals for one selected spike have been added to the histogram (Fig. 1*A*), a different spike from the same set of spike-trains is selected (Fig. 1*B*). The origin of the histogram is shifted to be aligned with the newly selected spike, and again all intervals with the spike-trains at the test SPL are tallied. This process is repeated so that every spike of

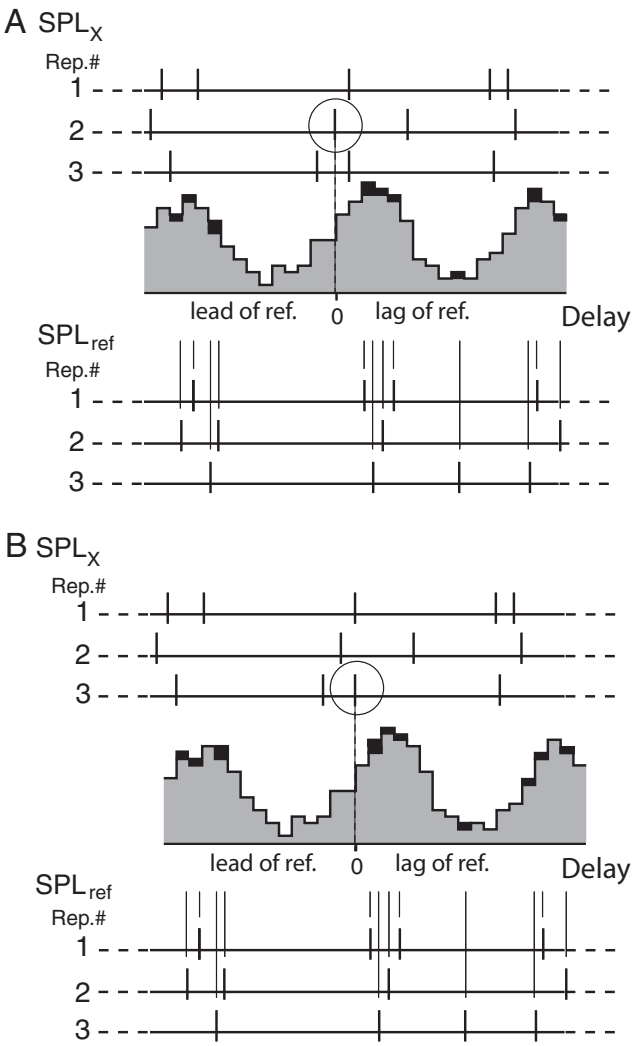

Figure 1. Schematic illustration of the correlogram calculation. ***A***, The 3 spike trains above the correlogram represent responses of a single fiber to stimulation with broadband noise at a variable intensity (SPL_X); the 3 spike trains at the bottom of the panel represent responses of the same fiber to the same stimulus at a reference intensity (SPL_{ref}). A spike is selected (circle) in the responses to SPL_X and all intervals between this spike and all spikes in response to SPL_{ref} are tallied in a histogram with a binwidth of 50 μs. Note that calculating these intervals is no different from determining whether two spikes, shifted in time by a certain delay, are coincident. For each coincidence or interval value, the corresponding histogram bin is increased by 1 (indicated in black). ***B***, A different spike is selected; the histogram is recentered so that the new spike represents 0 ms delay; and again all intervals between this new spike and spikes at SPL_{ref} are calculated. This process is repeated until all spikes to SPL_X have been used once. In the schematic, the spike train in response to SPL_X leads in time relative to SPL_{ref} which results in a shift of the correlogram to positive delays.

the responses at the SPL_X will function as zero time reference once. When comparing spike-trains obtained at the same SPL, the analysis is virtually identical except that identical spike-trains are excluded (a spike-train is never compared with itself), so as to avoid effects of the neural refractory period. The latter type of correlogram is referred to as the shuffled autocorrelogram. For the correlograms calculated across SPLs but within a single fiber, we simply use the term correlogram. Correlograms were normalized for average firing rate (in spikes/s), the number of stimulus repetitions and the stimulus duration, by dividing the number of coincidences by ($M^2 r^2 w D$) (where M is the number of stimulus repetitions, *r*, the average spike rate (in spikes/s), w, the window width, and D, the stimulus duration). For shuffled autocorrelograms, the normalization factor is [$M (M - 1) r^2 w D$].

The rationale of the entire procedure is that it predicts the output of a binaural coincidence detector receiving input from identical fibers on both sides. The correlograms show a basic similarity to binaural responses of ITD-sensitive neurons (Joris, 2003), and any latency changes resulting from changes in SPL should be visible as horizontal shifts of the correlogram.

Results

We first sketch basic possible outcomes of intensity on the correlograms using a simple model. We created a "left" and "right" input channel consisting of waveforms representing basilar membrane motion for a filter tuned to 500 Hz (following Mc Laughlin et al., 2007). The filter was identical for both channels and had a Gaussian amplitude spectrum with center frequency 500 Hz and width (defined as 2 SD of the Gaussian) of 150 Hz. When stimulated with identical white noise, the cross-correlation function of the output of these left and right channels shows a damped oscillatory pattern with a peak at zero delay and side peaks symmetrically positioned at positive and negative delays (Fig. 2*A*: since the output of both channels is identical, the function is effectively an autocorrelation function). The envelope of the correlogram, computed with the Hilbert transform (Hilbert function in Matlab, The MathWorks) and illustrated with a thin line, is also centered at zero delay. We then manipulated the timing relationship between the two channels by imposing specific relationships between their phase spectra. As is customary in binaural analyses (e.g., Yin and Kuwada, 1983b), these relationships are graphed as the interaural phase difference (IPD) as a function of frequency. The goal of these manipulations is to illustrate how changes in the phase spectrum affect the different features (fine-structure and envelope) of the cross-correlation function. For identical stimuli in the two channels (Fig. 2*A*), the IPD is 0 at all frequencies (top).

Figure 2*B–D* shows 3 examples where the phase spectrum was altered such that $IPD = mf + c$ (where *f* is frequency in Hz, *m* is the slope of the IPD function, and *c* is the Y-intercept at 0 Hz). The autocorrelation function and its envelope and IPD function (Fig. 2*A*) are always shown with thin lines, for reference. Figure 2*B* shows the cross-correlation function for a pure time delay of the right channel, where $c = 0$ and $m = 1$ ms. In this case, the cross-correlation function is identical to that in Figure 2*A*, but the entire function is shifted by 1 ms along the delay axis. Note that the fine-structure and the envelope of the cross-correlation function are equally delayed. On the other hand, if *c* is a constant and $m = 0$ ms, the envelope of the cross-correlation function remains centered at 0 ms, while the fine-structure is shifted within that envelope. The example (Fig. 2*C*) shows the special case of $c = -0.5$ cycle, which causes an inversion of fine-structure. Finally, Figure 2*D* shows the outcome when the IPD function "pivots" around the center frequency, i.e., where IPD is 0 at the center frequency but is changed in opposite ways for frequencies below and above. This occurs when the frequency-dependent and frequency-independent IPD contributions cancel at the center frequency: $mf = -c$. The example in Figure 2*D* shows the effect of a 1 ms delay combined with a 0.5 cycle shift: $IPD = 0.001 f - 0.5$. The resulting cross-correlation function shows a 1 ms shift in envelope but not in fine-structure.

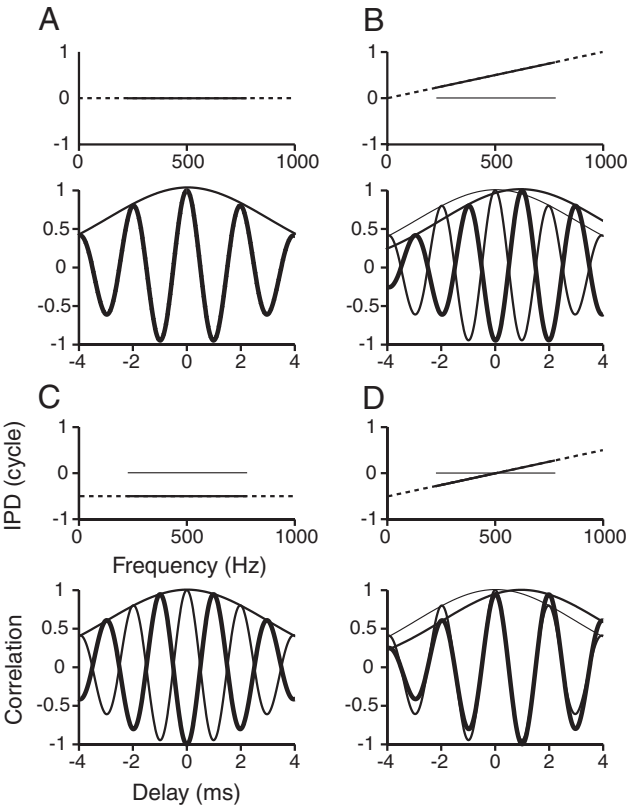

Figure 2. Simple model to illustrate the effect of interaural phase difference (IPD) on the cross-correlation function. The output of identical 150 Hz wide Gaussian filters centered at 500 Hz, in response to broadband noise, are cross-correlated. The phase spectrum of one input is kept constant across all four panels. The phase spectrum of the other "ear" is manipulated such that IPD varies linearly with frequency. ***A***, The phase spectra are identical (IPD = 0, top): the cross-correlation is effectively an autocorrelation, peaking at 0 ms (bottom). The thin line shows its envelope, obtained with the Hilbert transform, which also peaks at 0 ms. ***B***, Pure time delay: IPD is proportional to frequency *f* and equals 0.001 *f*, simulating a delay of 1 ms. The entire cross-correlation function is shifted by 1 ms: its fine-structure (bold line) and its envelope (thinner line). The correlation and IPD function of A are also shown for comparison. ***C***, Constant phase shift: IPD = 0.5 cycle. Shifting the phase of the impulse response of one "ear" by a half-cycle results in an inversion of the fine-structure of the cross-correlation function, without affecting its envelope. ***D***, Combination of a time shift (1 ms) and phase shift (−0.5 cycle), such that the IPD pivots at the filter's center frequency: IPD = 0.001*f* - 0.5. The cross-correlation function's envelope shifts by 1 ms, but not its fine-structure.

In what follows we will quantify both the fine-structure and envelope of the correlograms. If an increase in intensity corresponds to a simple time shift of the entire spike train to shorter latencies, as surmised by the latency hypothesis, the cross-correlogram of the responses to 2 different SPLs will be affected as in Figure 2*B* so that both fine-structure and envelope components of the correlograms are equally time shifted. On the other hand, if a change in stimulus intensity is accompanied by equal but opposite changes in phase above and below the center frequency, the correlogram fine-structure is unaffected but its envelope is time-shifted by an amount equaling the slope of the phase (IPD) function (Fig. 2*D*). This type of phase change has been observed in cochlear mechanics (Robles and Ruggero, 2001) and in AN responses (Anderson et al., 1971). Finally, if the effects

of changes in SPL would be identical at all CFs in units of phase, they would become smaller in units of time with increasing CF.

Delay measurements in single fibers

We first illustrate results for individual fibers and then present population results for the 232 AN fibers for which useful data were obtained. Figure 3*A*,*B* shows results for a fiber with low CF (521 Hz). Each thick line in the panels of column A shows a correlogram between two sets of spike-trains. One set is identical for all panels, namely the spike-trains recorded at 70 dB SPL (the "reference" SPL). The second set is different for each panel: top to bottom, it was recorded at a "test SPL" of 80, 70, 60, and 50 dB. Thus, each correlogram compares the spike timing of the same fiber in response to the same noise waveform presented at 2 SPLs. Despite the fact that all our data are monaural, we will refer to these comparisons as "ILD" conditions to facilitate the comparison with binaural data, and note them by the shorthand of 80|70, 70|70, 60|70 etc. Note that the 70|70 condition is special since it involves a comparison between spike-trains within a dataset, for which we use the shuffled autocorrelogram (Joris, 2003; Louage et al., 2004). Because we presented the same noise, at all SPLs, at two polarities, each correlogram is actually the average of two correlograms. For example, the top correlogram in Figure 3*A* (thick line) is the average of one correlogram for spike-trains to noise A+ at 80 and 70 dB, and one for spike-trains to noise A− at 80 and 70 dB.

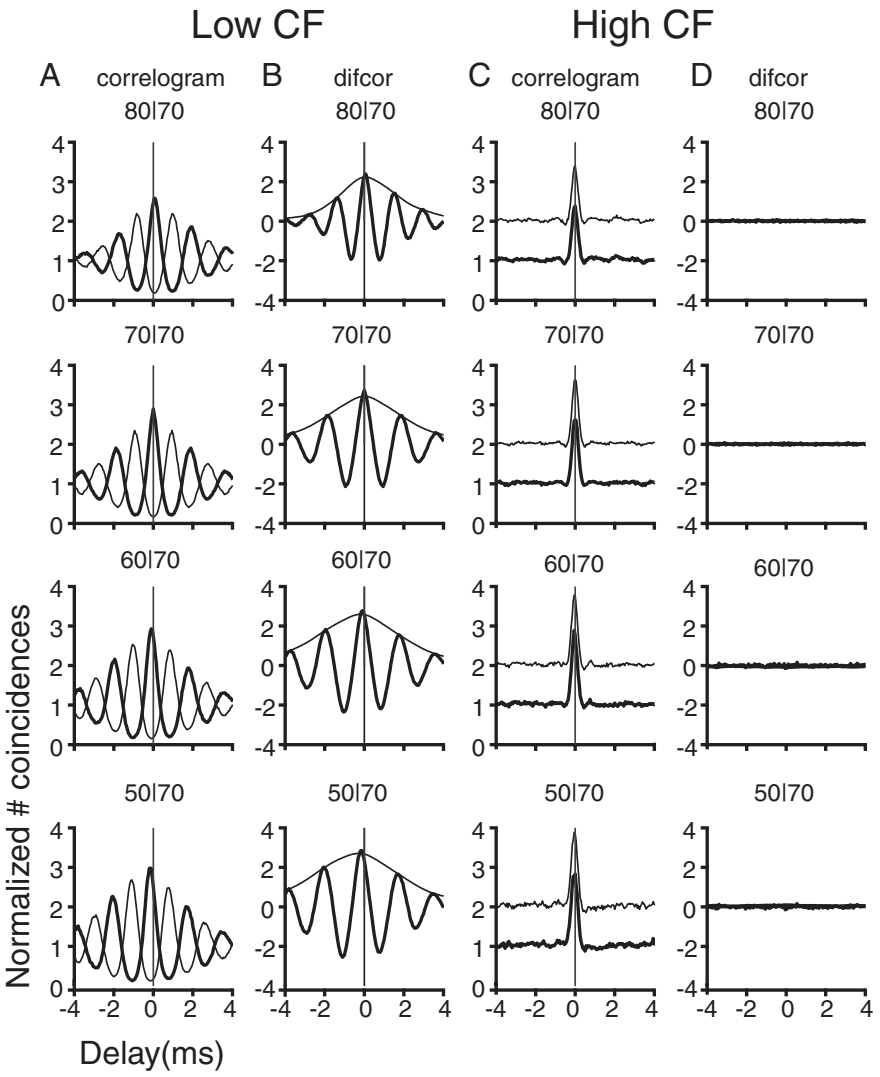

Figure 3. The ongoing timing of responses shows submillisecond shifts with increasing level. Examples of correlograms for a fiber with low CF (***A***, ***B***: CF = 521 Hz, SR = 71 spikes/s) and high CF (***C***, ***D***: 27 kHz, SR 0.4 spikes/s), using a reference SPL of 70 dB. ***A***, correlograms based on responses to correlated (bold line) and anticorrelated (thin line) noise pairs at different levels. Levels for each noise pair (e.g., 80|70) indicate test (e.g., 80) and reference (e.g., 70) level, respectively. Positive correlogram values indicate lag of the response at the reference SPL relative to the test SPL. At test levels higher than the reference (80|70, top) the response at the reference SPL slightly lags that at the test SPL, while the opposite is true at 60|70 and 50|70. The correlograms at 70|70 are autocorrelograms and peak at 0 delay. ***B***, Difcors calculated by subtracting the correlograms to anticorrelated noise from the correlograms to correlated noise. The thin line is an estimate of the envelope of the difcor calculated with the Hilbert transform. ***C***, ***D***, Identical analysis for the high-CF fiber. Abscissa labels of bottom left panel apply to all panels. Flat difcors (***D***) indicate that correlograms to correlated and anticorrelated noise are virtually identical: for clarity we offset the latter by one vertical unit in ***C***.

A cursory look across the correlograms in the left column (Fig. 3*A*) shows that the effects of SPL are subtle. The convention of the "ILD" notation and that of the delay axis are such that the association of a high test SPL (relative to the reference SPL) with a shift toward positive delays indicates a decrease in latency with increasing SPL. For example, the correlogram to 80|70 (Fig. 3*A*, top) shows a small lag: the central peak and sidepeaks are shifted in a positive delay direction when compared with the correlogram at 70|70, indicating that the increase of 10 dB causes a shortening of spike times. Vice versa, the correlogram to 50|70 (Fig. 3*A*, bottom) shows a small lead: the central peak and sidepeaks are shifted in a negative delay direction when compared with the correlogram at 70|70, indicating that the decrease of 20 dB causes an lengthening of spike times.

Figure 3*C* shows results for a fiber with high CF (27 kHz) for the same stimuli. While all correlograms in Figure 3*A* show a damped oscillatory pattern with a period close to the characteristic period (CF^{-1}, here ~2 ms), the correlograms in Figure 3*C* show a single peak. These differences in shape have been reported earlier (Joris, 2003; Louage et al., 2004) and are consistent with known peripheral auditory properties. At low CFs, the correlograms are dominated by the stimulus fine-structure. At CFs above the range of phase-locking to pure tones, the correlograms reflect phase-locking to the envelope. This envelope is not present as such in the broadband noise stimulus, but is imposed by the narrowband filtering (Rice, 1954) inherent in cochlear function (Joris, 2003). The damping of the oscillatory patterns (at low CFs) and the width of the single peaks (at high CFs) are dominated by the bandwidth of the cochlear filter (Mc Laughlin et al., 2007, 2008; Joris et al., 2008a). Because all correlograms in Figure 3 are normalized to the total number of spikes (see Methods, Coincidence analysis and general approach), they approach unity at large delay values. Unity indicates absence of correlation between the two sets of spike-trains. As in Figure 3*A*, the correlograms within the column (Fig. 3*C*) show only subtle differences.

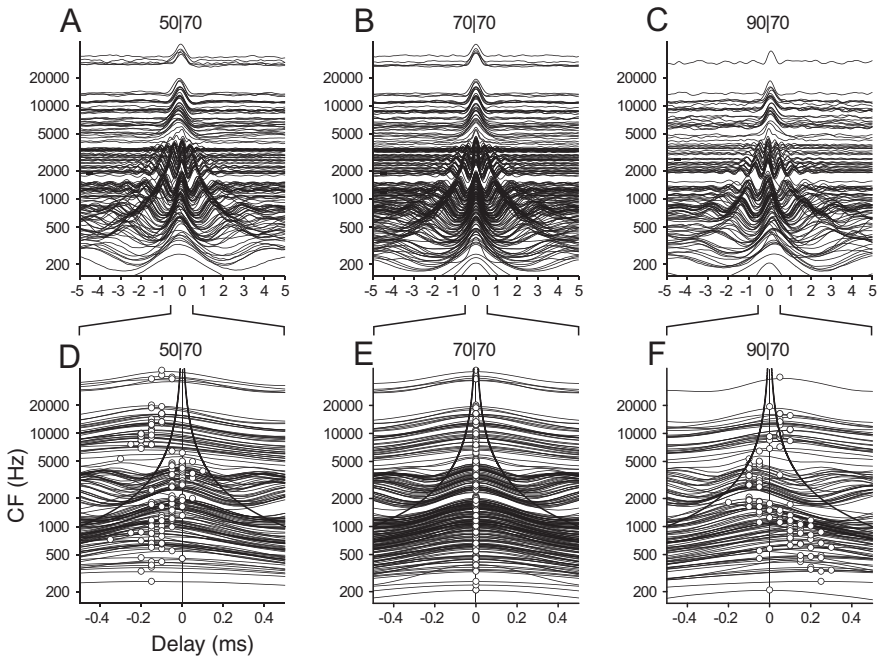

Figure 4. Correlograms for different "ILD" conditions (indicated above each panel) reveal subtle but systematic shifts across CF. The correlograms are normalized to their maximum, and are vertically stacked according to CF. ***A–C***, Correlograms over a 10 ms range of delays, for broadband noise presented at equal (***B***) or unequal (***A***, ***C***) SPL. There is a transition at CF ~ 3.8 kHz from a regime of coding of fine-structure to a regime of coding of envelope. ***D–F***, zoom-in on the central part of the correlograms. The primary peaks are marked by circles. In the autocorrelograms (***E***) all peaks occur at zero delay. Decrease of SPL (***D***) results in a lead (negative delay values) of the spikes to the reference SPL (70 dB) relative to the test SPL (50 dB); increase of SPL (***F***) results mostly in a lag (positive delay values) of the responses to the reference SPL (70 dB) relative to the test SPL (90 dB) but causes a lead in some fibers. The solid hyperbolic lines in ***D–F*** span one CF period.

The thin lines in Figure 3*A*, *C* also show correlograms to two sets of spike-trains at SPLs 80|70, 70|70, 60|70, and 50|70, but here the two sets are in response to noises of opposite polarity. For example, in the topmost panel of Figure 3*A* the thin line is the average of the correlogram for spike-trains to noise A+ at 80 dB and A− at 70 dB, and that to noise A− at 80 dB and A+ at 70 dB. Clearly, in the low-CF fiber (Fig. 3*A*), inverting the stimulus polarity causes an anticorrelation between spike trains, leading to an inversion in the correlogram (compare Fig. 2*C*). This is not the case for the high-CF fiber, where the correlogram is insensitive to stimulus polarity. Indeed, the correlograms to correlated and uncorrelated noise in Figure 3*C* are virtually identical and are offset by 1 unit on the ordinate, for clarity. The availability of correlograms to both correlated and anticorrelated noise allows us to disentangle effects of SPL on fine-structure and envelope. In the analysis of the coding of fine-structure in low CF fibers, the contribution of the envelope is minimized by subtracting the correlogram to anticorrelated noise from that to correlated noise, which results in difcors (Fig. 3*B*). For high CF fibers, the difcor is completely flat (Fig. 3*D*) because the correlograms are completely envelope-based and therefore independent of stimulus polarity.

The two examples of Figure 3 show that the correlation patterns are strikingly stable with stimulus intensity. Over the 30 dB range of SPLs covered in this figure, the temporal shifts are barely visible at the time scale of the figure. As will be illustrated in the next figure (Fig. 4), the shifts of the main peak are at most a few hundred μs, both in fine-structure and envelope. This is in stark contrast to the behavior of response onset latency, which can show millisecond shifts over this range of SPLs (Kiang et al., 1965; Kitzes et al., 1978; Hirsch et al., 1985; Heil and Irvine, 1997; Heil, 1998; Klug et al., 2000; Irvine et al., 2001). In addition to shifts of the entire correlogram along the abscissa, there are other effects of increases in SPL such as increased damping (Fig. 3*B*: secondary peaks are smaller at 80|70 than at 50|70) and smaller spacing between primary and secondary peaks (Fig. 3*B*: spacing is ~2 ms at 50|70 but <2 ms at 80|70). These changes are consistent with the decrease in frequency selectivity and change in center frequency with SPL (Louage et al., 2004; Joris et al., 2008a) but are not further discussed here. The magnitude of the correlograms is affected as well: this is discussed below (see Fig. 7).

Two regimes in the distribution of peak delay

To obtain an overview of the response of the entire AN to a given pair of SPL values for a single stimulus, we construct stacks of correlation functions. For example, Figure 4*A* shows the correlograms of all fibers studied for the 50|70 condition (including the two examples at 50|70 in Fig. 3*A*, *C*). All functions are normalized to their maximum and are vertically offset so that their asymptotic value of 1 intersects the ordinate at the fiber's CF. The upper row of panels (Fig. 4*A–C*) shows the correlograms for delays between ±5 ms; the lower row (Fig. 4*D–F*) displays the same data but zooms in on small delay values, between ±0.5 ms. For ease of viewing, the primary peaks are indicated by circles in the bottom panels.

The middle panels, for the 70|70 condition, are simply the autocorrelation functions for our entire sample of fibers. Note that the primary peak (defined as the maximum of the correlogram) of all functions lines up at 0 ms delay, within the limits of our 50 μs coincidence window. This is not so by necessity (see Fig. 8*J* in Joris et al., 2006b for a counter-example) and therefore gives confidence in the validity of our measure. As expected, the correlograms show an increase in the frequency of the periodicity with increasing CF, noticeable as a shift of the secondary peaks toward the primary peak. Above CF ~ 4000 Hz, the oscillatory pattern disappears and is replaced by a single peak. This transition indicates a change in temporal coding with CF, which is dominated by fine-structure at low CFs (as in Fig. 3*A*) and by envelope at high CFs (as in Fig. 3*C*) (Joris, 2003).

The left panels (Fig. 4*A*, *D*) show correlograms for a 20 dB level difference (50|70). Clearly, the 20 dB "ILD" causes shifts to negative delays, indicating that the spikes in the reference spike-train (at 70 dB) lead relative to the test spike-train (at 50 dB). The pattern is bimodal. Large shifts occur at the lowest CFs, where they amount to a few hundred microseconds. The shifts become smaller with increasing CF but increase again quite suddenly at CFs ~3–4 kHz, to then decrease again at higher CFs. For reference, the distance between the solid hyperbolic lines in Figure 4*D* equals the magnitude of the characteristic period (CF^{-1}). At low CFs, the shifts in primary peak are smaller than CF^{-1}, while at high CFs they are larger.

The right panels (Fig. 4*C*,*F*) show correlograms for a test SPL which is higher than the reference SPL (90|70). Here the primary peaks are mostly shifted to positive delays, indicating that the

reference spike-train (at 70 dB) lags relative to the test spike-train (at 90 dB). However, the pattern of shifts is more complex than in the leftmost panels: fibers at CFs of 800–3000 Hz shift in the opposite direction. Contrary to the latency–intensity relationship generally observed in sensory systems (e.g., Rose and Mountcastle, 1954; Cleland and Enroth-Cugell, 1970; Ikeda and Wright, 1972; Gawne et al., 1996; Reich et al., 2001; Cang and Isaacson, 2003; Sawtell et al., 2006), the responses at these CFs are delayed by an increase in intensity (from 70 to 90 dB), and we therefore refer to this shift as a "paradoxical shift."

The layout of Figure 4 is inspired by readouts in binaural models of human psychophysics (Lindemann, 1986; Stern et al., 1988; Colburn, 1996; Breebaart et al., 2001). Although each correlogram in Figure 4 is based on monaural responses recorded from a single AN fiber, we can consider each pair of spike-trains (recorded at 80|70, 70|70, etc.) as being derived from identical fibers in the left and right AN. Thus, each correlogram can be viewed as the output of a simple binaural coincidence detector with only two, anatomically identical, inputs. The stack of correlograms in Figure 4 then corresponds to the output of a population of coincidence detectors, fed by AN fibers of identical CF and SR on the two sides, in response to noise at 50|70, 70|70, 90|70 dB at the two ears. The delay on the abscissa of this plane indicates either the neural delays that the nervous system needs to supply to bring the spike trains in coincidence (also called "matching" or "internal" delays), or alternatively the stimulus ITD that needs to accompany the ILD to generate the maximal number of coincidences in the absence of an internal delay.

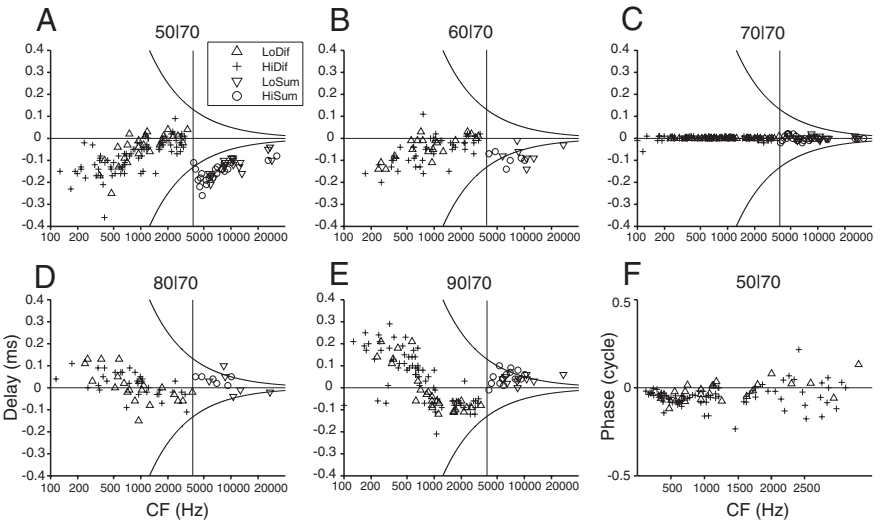

Figure 5. Shifts of correlogram peaks show two regimes in different CF regions. Primary peak shifts for 5 different "ILD" conditions (indicated above the panels), computed from difcors for low-CF fibers (<3.8 kHz, vertical line) and from sumcors for high-CF (>3.8 kHz) fibers. Different symbols are used to indicate the type of correlogram used (difcor vs sumcor) and to separate fibers with low and high SR: triangles and + at low CF, inverted triangles and circles at high CF. ***A***, ***B***, Stimulus levels below the 70 dB reference level result in a delay of the spikes in the test spike trains relative to the spikes in the reference spike trains. ***C***, Autocorrelograms are centered near 0 delay. ***D***, ***E***, High test levels result in shifts of both difcors and sumcors toward positive delay values, except in the region between 0.8 and 3.8 kHz, where paradoxical shifts toward negative delays are observed. ***F***, Difcor delays for low-CF fibers of ***A*** replotted on a phase ordinate. Average phase shift was −0.04 cycle. Legend in ***A*** and axis labels in ***D*** apply to ***A–E***. Distance between hyperboles in ***A–E*** indicates CF^{-1}.

In neural terms, the stability of the temporal code in the face of intensity changes is remarkable. The stack of correlograms in Figure 4*A–C* is only 1 ms wide and—at that scale—barely changes for a tenfold change in sound pressure in either direction. At the same time, the shifts are too large, at least at some CFs, to state that the spike timing patterns conveyed to the CNS are entirely invariant with ILD. Even though the shifts generated by an "ILD" are very small compared with the shifts reported for onset latency, their order of magnitude is similar to the ITDs that cats experience (approximately ±400 μs), so they may be relevant perceptually (see Discussion).

To quantify the trends in the raw correlograms of Figure 4, we simplify and refine our analysis in several ways. First, we simplify by reducing the position of the correlograms on the delay abscissa to a single number. Figure 5 shows the delay in the primary peak of the correlograms. We choose the primary peak because it is unambiguous and is the most important feature from a binaural point of view. Second, to maximize accuracy in the measurement of this delay, we combine correlograms for correlated and anticorrelated noise pairs. At low CFs, the correlograms are dominated by response fine-structure: here we quantify the temporal shift by measuring the delay of the primary peak of difcors (obtained by subtracting the correlograms for anticorrelated from those for correlated noise pairs, as in Fig. 3*B*). At high CFs, the correlograms are dominated by response envelope: here we quantify the temporal shift by measuring the delay of the peak of the sumcor (obtained by averaging the correlograms for correlated and anticorrelated noise pairs, as in Fig. 3*D*). For the vast majority of fibers, the raw correlograms were clearly dominated by either fine-structure or envelope. Fibers over a narrow range of intermediate CFs display a mix of fine-structure and envelope coding (Joris, 2003; Louage et al., 2004). To classify responses in this region of intermediate CFs, we used the measure of Louage et al. (2004, their Fig. 14) i.e., the peak value (at zero delay) of the correlogram to correlated noise (at 70|70), divided by the value at zero delay of the correlogram to anticorrelated noise. A ratio <0.5 indicates dominance of fine-structure, in which case we use the difcor; a ratio >0.5 indicates dominance of envelope, in which case we use the sumcor. In our present sample, all fibers with CF < 3.8 kHz showed dominance by fine-structure, and all fibers with CF > 3.8 kHz showed dominance by envelope. The vertical line at 3.8 kHz in Figures 5 and 6 indicates this transition. For the remainder of the paper, we will refer to those two groups as low-CF and high-CF fibers. Note that this division is made solely on the basis of the ratio just mentioned, calculated on the 70|70 autocorrelograms, and is thus made independently of the measurement of the delay of the primary peak. Third, to remove the 50 μs quantization in the measurement of delay (see Methods, Coincidence analysis and general approach), the difcors and sumcors were interpolated with a cubic spline. It is important to note that these 3 procedures allow better visualization but are not essential to our conclusions.

The trends described in Figure 4 are seen more clearly in Figure 5: CF dependence of the shift of the primary peak and the two regimes in this dependence (Fig. 5*A*); negative shifts for test levels lower than the reference level (50|70 and 60|70) (Fig. 5*A*,*B*) and mostly positive shifts for test levels higher than the reference level (80|70 and 90|70) (Fig. 5*D*,*E*); paradoxical shifts particularly at high sound levels (90|70) (Fig. 5*E*). In addition, Figure 5 shows

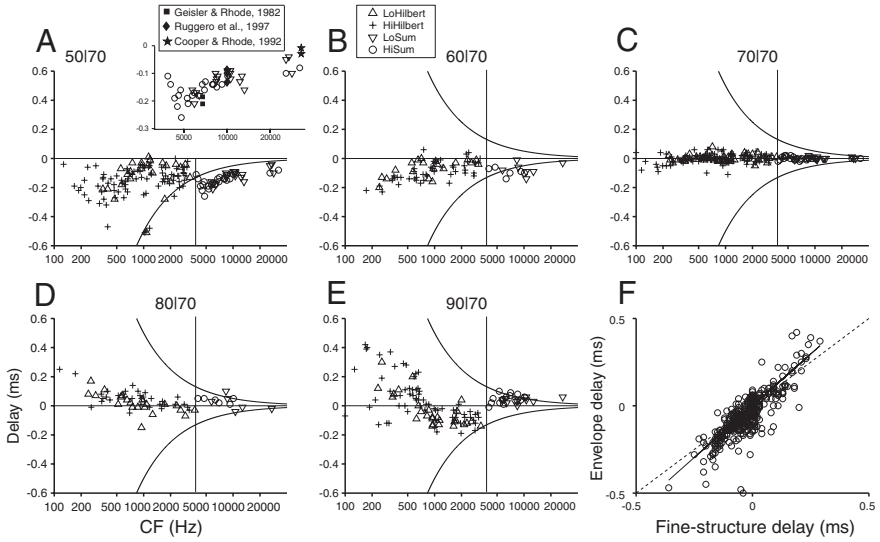

Figure 6. Shifts in the envelope of correlograms. ***A–E***, The correlogram delays at low CF are measured on the correlogram envelope obtained with the Hilbert transform (in low and high SR fibers: LoHilbert and HiHilbert). The data at high CF are the same as in Figure 5 and are the correlogram delays measured directly on the peak of the sumcor. Symbol caption in ***B*** applies to ***A–E***. The inset in ***A*** zooms in on the high CF data for a comparison with group delays taken from the literature (solid symbols). ***F***, In low-CF fibers, delays in correlogram envelope and fine-structure are well correlated. All stimulus conditions except 70|70 are included.

that shifts are larger for larger differences in sound levels (Fig. 5*A* vs *B*, *E* vs *D*), and that the shifts do not differ between low- and high-SR fibers (different symbols, boundary of 18 spikes/s). There is a remarkable and unexpected similarity in the pattern of CF-dependence at low and high CFs, i.e., in the timing of fine-structure and envelope, particularly in the 50|70 comparison (Fig. 5*A*): the shift decreases with CF both for fine-structure and envelope and has a similar magnitude and sign for the two forms of temporal coding, even though the data for fine-structure and envelope span different ranges of CF. Thus, at low CFs the shifts decrease from a maximum of a few hundred to 0 μs, following an approximately hyperbolic course, and the same applies to high CFs. Note, however, that paradoxical shifts at high SPL are only observed in the fine-structure and not in the envelope (Fig. 5*D*,*E*).

Figure 5*F* replots the low-CF data from Figure 5*A* on a phase ordinate (in cycles) by multiplying delay with CF. A clear, systematic dependence of phase on CF is not apparent, suggesting that the source of delay at these SPLs is close to a constant fraction of phase. The mean phase shift is −0.04 cycle.

Shifts in envelope delay across CF

As already mentioned, the striking and abrupt change in delay in Figures 4 and 5 coincides with the transition in the correlograms of the dominance of fine-structure or envelope. Even for correlograms that are dominated by fine-structure, an envelope can be defined using the Hilbert transform on the difcors (Joris et al., 2008a), as illustrated in Figure 3*B* (thin lines). This allows us to examine whether the trend observed in the (envelope-dominated) correlograms at high CFs continues into the low-CF range. Figure 6*A–E* shows the distribution of the delays in the maxima of the envelopes extracted with the Hilbert transform from difcors at low CF, together with the sumcor-based envelope delays at high CFs which were also shown in Figure 5. Note that the envelopes at low CFs are broad (see Fig. 3*B*) and not as clearly defined as at high CFs (Fig. 3*C*): this is visible in the scatter in delay for the autocorrelograms (compare Fig. 6*C* with Fig. 5*C*). Our expectation was that the trend for high-CF fibers would continue toward low CFs, i.e., an increase in the magnitude of delay along a hyperbolic trajectory, because all measures are now envelope-based. Surprisingly, the resulting delay distributions are not too different from the ones shown in Figure 5, indicating that at low CFs the delays of fine-structure and envelope are similar, suggesting that a change in SPL introduces a pure time delay (Fig. 2*B*). Figure 6*F* compares delay in fine-structure and envelope directly for low-CF fibers. All "ILD" stimulus conditions are included here (50|70, 60|70, 80|70 and 90|70), excluding autocorrelations (70|70). Delays in fine-structure and envelope are well correlated ($r = 0.8$); the relationship is steeper than, and significantly differs from, the line of equality ($p < 0.001$, slope of linear regression = 1.15) i.e., changes in SPL cause a slightly larger delay in the envelope than in the fine-structure.

That the similarity in delay between fine-structure and envelope in low-CF fibers is not some artifact of our analysis can also be appreciated from the fact that the basic shape of the correlograms remains largely unaffected by "ILD". As illustrated in Figure 2, it is only for a pure time delay (Fig. 2*B*), that the overall shape of the cross-correlation function is unaffected and that the relationship of the fine-structure to the envelope is unaltered, since both are shifted by an equal amount on the delay axis. This is also seen in the correlograms in Figure 3*A*,*B*. For example, the size of the secondary peak at negative delays is very similar to that at positive delays at all "ILDs."

Cochlear mechanical data, against which the neural delays measured here can be compared, are available at high CFs. We calculated the change in slope of the phase spectra (group delay) from published cochlear mechanical measurements over a 20 dB change in stimulus level, for CFs of 6.8 kHz (Geisler and Rhode, 1982, squirrel monkey); 10 kHz (Ruggero et al., 1997, chinchilla); and 33 kHz (Cooper and Rhode, 1992, cat). The resulting values are shown in the inset of Figure 6*A* (solid symbols): they are in good agreement with our neural data, which are also replotted in the inset. A change that is constant in units of phase predicts a hyperbolic decrease in time with increasing CF. This pattern fits the neural and mechanical observations at high CFs, but remarkably it does not smoothly extend to the envelope delays at low CFs, which are much smaller than predicted by an extrapolation of the trend at high CFs toward low CFs. Thus, while for high-CF fibers the decrease in latency of ongoing spikes with SPL may simply reflect the change in mechanical group delay, it is unclear whether this applies to low CFs. Unfortunately, mechanical measurements at the cochlear apex are scant due to its inaccessibility, which hampers an interpretation of the neural data in terms of mechanical events.

Effects of SPL on correlogram magnitude

So far, we have focused on temporal shifts of the correlograms, but it is to be expected that their magnitude will also be affected by SPL. Figure 7*A*,*B* shows that this is indeed the case. Each datapoint shows the correlation index (CI, see Joris et al., 2006b), i.e., the maximum of the normalized correlogram (Fig. 3*A*,*C*, thick lines), as a function of "ILD". The reference SPL was 70 dB.

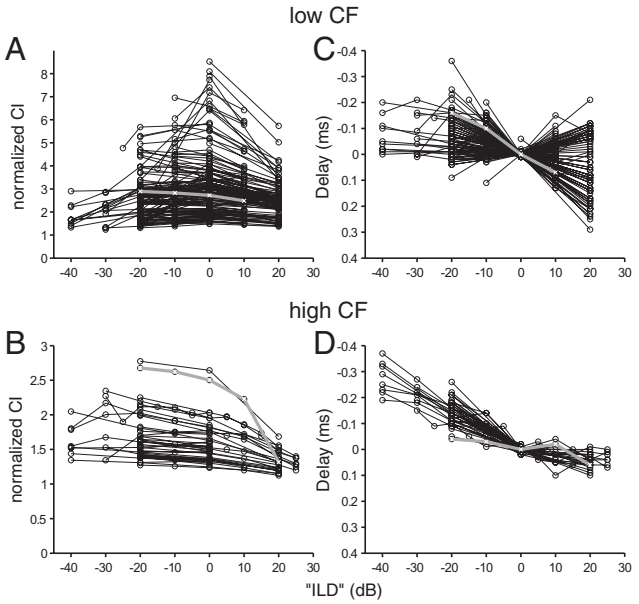

Figure 7. Dependence of correlogram magnitude and delay on "ILD". Abscissa: "ILD", using 70 dB SPL as reference. Upper panels are for fibers with CF < 3.8 kHz. Lower panels are for fibers with CF > 3.8 kHz. ***A***, ***B***, Ordinate: correlation index (CI) i.e., the maximum of the correlogram normalized for the number of spikes. CI = 1 indicates the number of coincidences as expected from chance. Each line joins measurements on one fiber. While the CI tends to be maximum at 0 "ILD" in low-CF fibers, it decreases with increasing "ILD" in high-CF fibers. Note the difference in ordinate scale between ***A*** and ***B***. ***C***, ***D***, Ordinate: delay of the primary peak of the correlogram. Negative values (i.e., lead of the reference level of 70 dB SPL) are plotted upward. At negative "ILD", i.e., lower SPL than the reference SPL of 70 dB, the responses at 70 dB generally lead relative to the (lower) test SPL. At positive "ILD" the responses at 70 dB generally lag relative to the (higher) test SPL, but at low CFs (***C***) many "paradoxical" latency shifts are observed. The data highlighted with a thick gray line and white "x" symbols illustrate measurements for the two fibers of Figure 3. The data are calculated on splined difcors for the low CF data (***A***, ***C***, $N = 175$ fibers) and on splined sumcors for the high CF data (***B***, ***D***, $N = 40$ fibers).

Data points from the same fiber are joined by a line. For illustration, the CIs for the low- and high-CF fiber of Figure 3*A*,*C* are shown with a thick gray line. In low-CF fibers (Fig. 7*A*), the autocorrelation ("ILD" = 0) tends to show the largest CI value, while in high-CF fibers (Fig. 7*B*), the values systematically decrease with increasing "ILD". Both trends are as expected. The coding by nerve fibers of the envelope in sinusoidally amplitude-modulated tones is strongly level-dependent (Smith and Brachman, 1980; Joris and Yin, 1992; Cooper et al., 1993). This also applies to responses to broadband noise (Louage et al., 2004): the CI decreases monotonically with SPL. So it is not surprising that spike times of responses at e.g., 70 dB are more tightly correlated with spike times at a lower SPL than at the same or a higher SPL (Fig. 7*B*), since spike timing is tighter at low SPL than at high SPL. In contrast, the coding of fine structure is more stable with SPL. Difcor peak values decrease only slightly with increasing level (Louage et al., 2004), and there is no reason to expect systematically higher correlations across spike trains at different SPLs than across spike trains to the same SPL. On the contrary, changes of filter bandwidth and center frequency with SPL cause some decorrelation between different SPLs, as commented higher in the discussion of Figure 3.

While Figures 4 and 5 provide a population overview of changes in delay for a given change in SPL, it is also of interest to examine the effects for a wider range of SPLs on individual fibers. To ease comparison with onset latency functions as they are routinely plotted (Kitzes et al., 1978; Heil and Irvine, 1997) we plot negative shifts (lag for the test condition) upward so that a decrease in latency for increasing SPL generates a negatively sloping function. The curves in Figure 7*C*,*D* show indeed a decrease in latency with increasing SPL, i.e., the changes in ongoing spike timing are generally in the same direction as the classical change in onset latency. Nevertheless there are several quantitative and qualitative differences. As pointed out higher (Figs. 3–5), the effects on ongoing timing are small (<0.5 ms over the 60 dB range tested). Also, in some low-CF fibers the curves are nonmonotonic and show an increasing lag at positive "ILD" values (Fig. 7*C*): these are the paradoxical shifts mentioned higher. Finally, even for low-CF fibers with monotonically decreasing curves, the shape of the curves differs from that of traditional onset latency curves: onset latency typically decreases steeply with increasing level at low suprathreshold levels and asymptotes at high levels, while in low-CF fibers there is little change in lag at low SPLs (at "ILDs" of −40 to −20). Individual curves of Figure 7*C* therefore tend to show an upward convexity rather than upward concavity. For high-CF fibers (Fig. 7*D*), the shape is closer to that of onset latency curves, being monotonically decreasing and upward concave.

Our choice of using the spike-trains at 70 dB (Figs. 3–7) as reference is arbitrary. To examine how this choice affects the delay measurements, we calculated correlograms for different reference levels (data not shown). The patterns illustrated in previous figures are unaffected by the choice of reference SPL. In fact, the delays between SPLs add almost linearly so that the delay for e.g., the 30|70 condition tends to equal the sum of the delays for the 30|40, 40|50, 50|60 and 60|70 conditions.

Discussion

We examined the effect of intensity on peripheral temporal coding to ongoing broadband noise. Previous studies mostly reported response phase to periodic stimuli, providing much detail on transfer functions but little overview across the AN. We applied a coincidence analysis to responses to a single stimulus to generate overviews of spike timing across AN fibers for a given change in intensity. Ongoing timing is strikingly stable: shifts are < 500 μs over a range of 60 dB (a 1000-fold change in sound pressure) (Fig. 7*C*,*D*). They depend on CF with a bimodal hyperbolic pattern: large temporal shifts at very low CFs which decrease with increasing CF, and an abrupt increase at 3.8 kHz followed again by a decrease (Figs. 4, 5). The transition coincides with that between phase-locking to fine-structure and envelope.

Origin of time shifts

For high CF fibers, the changes in timing are consistent with cochlear mechanical measurements (and sparse neural data: van der Heijden and Joris, 2003; Recio-Spinoso et al., 2005) which show decreasing group delay, i.e., a change in the slope of the phase spectrum (Fig. 2*B*,*D*), accompanying the decrease in frequency selectivity with increasing intensity (for review, see Robles and Ruggero, 2001). For the basal cochlea, where spatial scaling invariance is a reasonable approximation (Shera et al., 2000), changes that are constant in units of phase across CF predict a hyperbolic decrease in time with increasing CF. This pattern is observed and fits with delays calculated from cochlear mechanical measurements. Thus, for high-CF fibers the decrease in latency of ongoing spikes with SPL may simply reflect the change in mechanical group delay. Of course, spiking in AN fibers is delayed relative to the mechanical events due to transduction, synaptic transmission, and spike conduction, but if this delay is independent of SPL and CF (Ruggero and Rich, 1987), it

will not affect the distributions obtained from the correlograms. Note that, because of the absence of phase-locking to fine-structure, our high-CF neural data cannot distinguish between the two mechanisms illustrated in Figure 2*B*,*D*, but mechanical measurements show phase "pivoting" (Robles and Ruggero, 2001) so the scheme of Figure 2*D* is more likely.

The results at low CFs are more surprising and harder to interpret. We first consider the pattern expected if phase changes as in Figure 2*D* apply to low CFs, assuming that tuning along the cochlea varies only in center frequency and not in other properties. First, the correlogram fine-structure should not shift with SPL: its peak should remain centered at 0 ms or at integral multiples of CF^{-1}. Second, the envelope of the correlograms should shift due to a decrease in group delay and these shifts should smoothly extend the hyperbolic trajectory of delays at high CFs, which are *de facto* envelope-based. Neither of these two predictions is met (Figs. 5, 6*A*). Admittedly, a realistic prediction of the effects of SPL would be much more complex due to changes with CF in the sharpness of tuning; in the dependence of this sharpness on SPL; and in the dependence of the phase spectrum on SPL. Moreover, mechanically these factors are insufficiently known for the cochlear apex. Nevertheless, the patterns we observe are not in support of the pivoting phase scheme of Figure 2*D*. Rather, the similarity at low CFs of the delays in envelope and fine-structure (Fig. 6*F*) are akin to the effects of a pure time delay (Fig. 2*B*).

How do these observations fit with previous neural measurements? A classic study in squirrel monkey AN (Anderson et al., 1971) showed phase lags with increasing intensity for frequencies < CF, and phase leads for frequencies > CF (phase pivoting, Fig. 2*D*). This account is consistent with filter theory; with the broadening of frequency tuning; and with mechanical measurements at high CFs, and has been replicated in many species, including cat (Allen, 1983; Carney and Yin, 1988). However, recent studies show complex and less stereotyped phase changes, and the agreement with mechanical measurements is debated (van der Heijden and Joris, 2006; Palmer and Shackleton, 2009; Temchin and Ruggero, 2010; Versteegh et al., 2011). In fact, given the variability in these previous reports, the pattern of delays we find is surprisingly orderly.

An entirely different interpretation of the similarity in the hyperbolic relationship between delay and CF at high and low CF (Fig. 5*A*), more in line with the latency hypothesis, is based on the effective waveform driving spiking in AN fibers. At CFs where the correlograms have wide central peaks (e.g., at 500 Hz and 5 kHz, Fig. 4), the shifts in timing due to SPL are also largest, whereas at CFs with narrow central peaks (e.g., 2 kHz and 20 kHz), the shifts are small. Indeed, the relationship between magnitude of delay and width of the correlogram is similar in low and high CF regimes (data not shown). The bimodal pattern of Figure 5*A* perhaps arises postmechanically: temporal fluctuations in presynaptic and postsynaptic potentials, combined with a fixed threshold, may generate a frequency-dependent time shift in spiking. In the fine-structure regime, an increase in CF would translate into a decreasing time delay (effectively a phase shift) (Green, 1976). Fluctuations in envelope, induced by cochlear filtering (Joris, 2003), replace fine-structure at CFs above a few kHz and are dictated by filter bandwidth rather than CF. This bandwidth is narrow at the point of transition near 3.8 kHz, resulting in slow fluctuations, but widens with CF, resulting in faster envelope modulations (Joris and Yin, 1992) which would generate spiking with less delay. Postmechanical factors in AN timing are also surmised by Versteegh et al. (2011) and Heil and colleagues (Heil and Irvine, 1997; Heil and Neubauer, 2001; Heil, 2004) and a discontinuity in the trend of response latency with CF is also observed in Recio-Spinoso et al. (2005; their Fig. 15*A*). The latter study also reveals large shifts in phase (but not group) delay at high SPL, which likely explains the paradoxical shifts that we observed (Figs. 5, 6).

Together, the available evidence indicates that cochlear mechanical factors contribute to effects of intensity on neural timing, but it is unclear whether they explain the pattern across CF. More mechanical data of apical tuning are required to disentangle mechanical and postmechanical mechanisms. Note that most discussions of the "latency hypothesis" refer to neural thresholding rather than to cochlear mechanical mechanisms. It is remarkable to observe the overall (though not quantitative) similarity between latency functions as traditionally measured to stimulus onset, and the ongoing timing measured with correlograms (Fig. 7*C*,*D*), because the two sets of data likely involve very different mechanisms.

Relevance for perception

Whether the temporal shifts reported here have perceptual consequences is unclear. The largest effects are in CF regions (<1 kHz and ~5 kHz) where they are least likely to have binaural perceptual impact. Acoustic head shadow diminishes for decreasing frequency. For cats, the ILD at the lowest frequency reported (1 kHz (Tollin and Koka, 2009)) was maximally 9 dB. The ILD is presumably only a few dB at frequencies of a few hundred Hz, which would translate to a temporal shift of maximally a few tens of μs (Fig. 6*A*). However, in addition to the uncertainty regarding the magnitude of ILD and ITD at very low frequencies, effects of distance, ground plane, and body position are understudied and may render the binaural cues significantly larger than traditionally assumed (Brungart et al., 1999; Brungart and Rabinowitz, 1999; Kim et al., 2010). At CFs ~5 kHz, ILDs can reach magnitudes of the order tested here (Irvine, 1987; Musicant et al., 1990; Rice et al., 1992; Tollin and Koka, 2009) and could thus generate delays of a few hundred μs. However, timing at those CFs is dominated by envelope fluctuations, both monaurally and binaurally (Joris, 2003; Devore and Delgutte, 2010), which are less powerful than fine-structure in affecting the spatial percept (Wightman and Kistler, 1992; Macpherson and Middlebrooks, 2002). At these CFs, the direct effect of ILD on spike rate (via a subtractive binaural interaction) is more powerful than its indirect effect (via timing) (Joris and Yin, 1995; Joris, 1996). Overall, it appears unlikely that the effects of SPL on ongoing timing are a significant factor in spatial hearing.

The "latency hypothesis" as stated by Jeffress (1948) is a brief description of an idea, insufficiently precise to refute. The core idea is a peripheral conversion of intensity to time. Previous studies have shown the merit of this idea in understanding sensitivity to ILDs in transient responses at high CFs (Hirsch et al., 1985; Yin et al., 1985; Pollak, 1988; Park et al., 1996; Irvine et al., 2001). Sustained responses at low and high CFs can also be influenced by both ITD and ILD (Goldberg and Brown, 1969; Kuwada and Yin, 1983; Yin and Kuwada, 1983a; Yin and Chan, 1990; Finlayson and Caspary, 1991; Batra et al., 1993; Joris and Yin, 1995; Viete et al., 1997; Tollin and Yin, 2005; Palmer et al., 2007), but whether a peripheral cue conversion contributes to this interaction is less clear. Moreover, the interaction reported is often in a direction opposite to Jeffress' proposal. Psychophysical studies also fail to unequivocally support the latency hypothesis.

In conclusion, intensity changes cause small but systematic and CF-dependent shifts in the timing of sustained responses to

broadband noise. Because the nerve provides the auditory input to the CNS, all central monaural and binaural processing is potentially affected by these shifts. Compared with other sensory systems and to onset latency, the effects of intensity on ongoing timing are minute and perhaps contribute to the behavioral invariance that is present for most monaural and binaural attributes. But one can take the opposite view: the effects are small but systematic and may be exploited by the system e.g., to derive intensity information (Carney, 1994).

References

Adrian E (1928) The basis of sensation: the action of the sense organs. New York: WW Norton.

Allen JB (1983) Magnitude and phase-frequency response to single tones in the auditory nerve. J Acoust Soc Am 73:2071–2092.

Anderson DJ, Rose JE, Hind JE, Brugge JF (1971) Temporal position of discharges in single auditory nerve fibers within the cycle of a sine-wave stimulus: frequency and intensity effects. J Acoust Soc Am 49 [Suppl 2]:1131–1139.

Batra R, Kuwada S, Stanford TR (1993) High-frequency neurons in the inferior colliculus that are sensitive to interaural delays of amplitude-modulated tones: evidence for dual binaural influences. J Neurophysiol 70:64–80.

Breebaart J, van de Par S, Kohlrausch A (2001) Binaural processing model based on contralateral inhibition. I. Model structure. J Acoust Soc Am 110:1074–1088.

Brugge JF, Reale RA, Hind JE (1996) The structure of spatial receptive fields of neurons in primary auditory cortex of the cat. J Neurosci 16:4420–4437.

Brungart DS, Rabinowitz WM (1999) Auditory localization of nearby sources. Head-related transfer functions. J Acoust Soc Am 106:1465–1479.

Brungart DS, Durlach NI, Rabinowitz WM (1999) Auditory localization of nearby sources. II. Localization of a broadband source. J Acoust Soc Am 106:1956–1968.

Buell TN, Trahiotis C, Bernstein LR (1991) Lateralization of low-frequency tones: relative potency of gating and ongoing interaural delays. J Acoust Soc Am 90:3077–3085.

Cang J, Isaacson JS (2003) In vivo whole-cell recording of odor-evoked synaptic transmission in the rat olfactory bulb. J Neurosci 23:4108–4116.

Carney LH (1994) Spatiotemporal encoding of sound level: models for normal encoding and recruitment of loudness. Hear Res 76:31–44.

Carney LH, Yin TC (1988) Temporal coding of resonances by low-frequency auditory nerve fibers: single-fiber responses and a population model. J Neurophysiol 60:1653–1677.

Chase SM, Young ED (2007) First-spike latency information in single neurons increases when referenced to population onset. Proc Natl Acad Sci U S A 104:5175–5180.

Cleland BG, Enroth-Cugell C (1970) Quantitative aspects of gain and latency in the cat retina. J Physiol 206:73–91.

Colburn HS (1996) Computational models of binaural processing. In: Auditory computation (Hawkins H, McMullen T, eds), pp 332–400. New York: Springer.

Cooper NP, Rhode WS (1992) Basilar membrane mechanics in the hook region of cat and guinea-pig cochleae: sharp tuning in the absence of baseline shifts. Hear Res 63:163–190.

Cooper NP, Robertson D, Yates GK (1993) Cochlear nerve fiber responses to amplitude-modulated stimuli: variations with spontaneous rate and other response characteristics. J Neurophysiol 70:370–386.

Devore S, Delgutte B (2010) Effects of reverberation on the directional sensitivity of auditory neurons across the tonotopic axis: influences of interaural time and level differences. J Neurosci 30:7826–7837.

Durlach NI, Colburn HS (1978) Binaural phenomena. In: Handbook of perception, Ed 4 (Carterette E, Friedman M, eds), pp 365–465. New York: Academic.

Finlayson PG, Caspary DM (1991) Low-frequency neurons in the lateral superior olive exhibit phase-sensitive binaural inhibition. J Neurophysiol 65:598–605.

Furukawa S, Xu L, Middlebrooks JC (2000) Coding of sound-source location by ensembles of cortical neurons. J Neurosci 20:1216–1228.

Gaik W (1993) Combined evaluation of interaural time and intensity differences: psychoacoustic results and computer modeling. J Acoust Soc Am 94:98–110.

Gawne TJ, Kjaer TW, Richmond BJ (1996) Latency: another potential code for feature binding in striate cortex. J Neurophysiol 76:1356–1360.

Geisler CD, Rhode WS (1982) The phases of basilar-membrane vibrations. J Acoust Soc Am 71:1201–1203.

Goldberg JM, Brown PB (1969) Response of binaural neurons of dog superior olivary complex to dichotic tonal stimuli: some physiological mechanisms of sound localization. J Neurophysiol 22:613–636.

Gollisch T, Meister M (2008) Rapid neural coding in the retina with relative spike latencies. Science 319:1108–1111.

Green D (1976) An introduction to hearing. Hillsdale: Lawrence Erlbaum.

Heil P (1998) Neuronal coding of interaural transient envelope disparities. Eur J Neurosci 10:2831–2847.

Heil P (2004) First-spike latency of auditory neurons revisited. Curr Opin Neurobiol 14:461–467.

Heil P, Irvine DR (1997) First-spike timing of auditory-nerve fibers and comparison with auditory cortex. J Neurophysiol 78:2438–2454.

Heil P, Neubauer H (2001) Temporal integration of sound pressure determines thresholds of auditory-nerve fibers. J Neurosci 21:7404–7415.

Hirsch JA, Chan JC, Yin TC (1985) Responses of neurons in the cat's superior colliculus to acoustic stimuli. I. Monaural and binaural response properties. J Neurophysiol 53:726–745.

Ikeda H, Wright MJ (1972) Receptive field organization of 'sustained' and 'transient' retinal ganglion cells which subserve different function roles. J Physiol 227:769–800.

Irvine DR (1987) Interaural intensity differences in the cat: Changes in sound pressure level at the two ears associated with azimuthal displacements in the frontal horizontal plane. Hear Res 26:267–286.

Irvine DR, Park VN, McCormick L (2001) Mechanisms underlying the sensitivity of neurons in the lateral superior olive to interaural intensity differences. J Neurophysiol 86:2647–2666.

Jeffress LA (1948) A place theory of sound localization. J Comp Physiol Psychol 41:35–39.

Johansson RS, Birznieks I (2004) First spikes in ensembles of human tactile afferents code complex spatial fingertip events. Nat Neurosci 7:170–177.

Joris PX (1996) Envelope coding in the lateral superior olive. II. Characteristic delays and comparison with responses in the medial superior olive. J Neurophysiol 76:2137–2156.

Joris PX (2003) Interaural time sensitivity dominated by cochlea-induced envelope patterns. J Neurosci 23:6345–6350.

Joris PX, Smith PH (1998) Temporal and binaural properties in dorsal cochlear nucleus and its output tract. J Neurosci 18:10157–10170.

Joris PX, Yin TC (1992) Responses to amplitude-modulated tones in the auditory nerve of the cat. J Acoust Soc Am 91:215–232.

Joris PX, Yin TC (1995) Envelope coding in the lateral superior olive. I. Sensitivity to interaural time differences. J Neurophysiol 73:1043–1062.

Joris PX, Van de Sande B, Louage DH, van der Heijden M (2006a) Binaural and cochlear disparities. Proc Natl Acad Sci U S A 103:12917–12922.

Joris PX, Louage DH, Cardoen L, van der Heijden M (2006b) Correlation index: a new metric to quantify temporal coding. Hear Res 216–217:19–30.

Joris PX, Louage DH, van der Heijden M (2008a) Temporal damping in response to broadband noise. II. Auditory nerve. J Neurophysiol 99:1942–1952.

Joris PX, Michelet P, Franken TP, McLaughlin M (2008b) Variations on a Dexterous theme: peripheral time-intensity trading. Hear Res 238:49–57.

Kiang NY, Watanabe T, Thomas EC, Clark LF (1965) Discharge patterns of single fibers in the cat's auditory nerve, Research Monograph 35. Cambridge, MA: MIT Press.

Kim DO, Bishop B, Kuwada S (2010) Acoustic cues for sound source distance and azimuth in rabbits, a racquetball and a rigid spherical model. J Assoc Res Otolaryngol 11:541–557.

Kitzes LM, Gibson MM, Rose JE, Hind JE (1978) Initial discharge latency and threshold considerations for some neurons in cochlear nuclear complex of the cat. J Neurophysiol 41:1165–1182.

Klug A, Khan A, Burger RM, Bauer EE, Hurley LM, Yang L, Grothe B, Halvorsen MB, Park TJ (2000) Latency as a function of intensity in auditory neurons: influences of central processing. Hear Res 148:107–123.

Kuwada S, Yin TC (1983) Binaural interaction in low-frequency neurons in inferior colliculus of the cat. I. Effects of long interaural delays, intensity,

and repetition rate on interaural delay function. J Neurophysiol 50:981–999.
Lindemann W (1986) Extension of a binaural cross-correlation model by contralateral inhibition. I. Simulation of lateralization for stationary signals. J Acoust Soc Am 80:1608–1622.
Louage DH, van der Heijden M, Joris PX (2004) Temporal properties of responses to broadband noise in the auditory nerve. J Neurophysiol 91:2051–2065.
Macpherson EA, Middlebrooks JC (2002) Listener weighting of cues for lateral angle: the duplex theory of sound localization revisited. J Acoust Soc Am 111:2219–2236.
Mc Laughlin M, Van de Sande B, van der Heijden M, Joris PX (2007) Comparison of bandwidths in the inferior colliculus and the auditory nerve. I. Measurement using a spectrally manipulated stimulus. J Neurophysiol 98:2566–2579.
Mc Laughlin M, Chabwine JN, van der Heijden M, Joris PX (2008) Comparison of bandwidths in the inferior colliculus and the auditory nerve. II: Measurement using a temporally manipulated stimulus. J Neurophysiol 100:2312–2327.
Moller AR (1975) Latency of unit responses in cochlear nucleus determined in two different ways. J Neurophysiol 38:812–821.
Musicant AD, Chan JC, Hind JE (1990) Direction-dependent spectral properties of cat external ear: new data and cross-species comparisons. J Acoust Soc Am 87:757–781.
Palmer AR, Shackleton TM (2009) Variation in the phase of response to low-frequency pure tones in the guinea pig auditory nerve as functions of stimulus level and frequency. J Assoc Res Otolaryngol 10:233–250.
Palmer AR, Liu LF, Shackleton TM (2007) Changes in interaural time sensitivity with interaural level differences in the inferior colliculus. Hear Res 223:105–113.
Park TJ, Grothe B, Pollak GD, Schuller G, Koch U (1996) Neural delays shape selectivity to interaural intensity differences in the lateral superior olive. J Neurosci 16:6554–6566.
Pollak GD (1988) Time is traded for intensity in the bat's auditory system. Hear Res 36:107–124.
Recio-Spinoso A, Temchin AN, van Dijk P, Fan YH, Ruggero MA (2005) Wiener-kernel analysis of responses to noise of chinchilla auditory-nerve fibers. J Neurophysiol 93:3615–3634.
Reich DS, Mechler F, Victor JD (2001) Temporal coding of contrast in primary visual cortex: when, what, and why. J Neurophysiol 85:1039–1050.
Rice JJ, May BJ, Spirou GA, Young ED (1992) Pinna-based spectral cues for sound localization in cat. Hear Res 58:132–152.
Rice SO (1954) Mathematical analysis of random noise. In: Selected papers on noise and stochastic processes (Wax N, ed), pp 133–162. New York: Dover.
Rieke F, Warland D, de Ruyter van Steveninck R, Bialek W (1997) Spikes: exploring the neural code. Cambridge, MA: MIT Press.
Robles L, Ruggero MA (2001) Mechanics of the mammalian cochlea. Physiol Rev 81:1305–1352.
Rose JE, Mountcastle VB (1954) Activity of single neurons in the tactile thalamic region of the cat in response to a transient peripheral stimulus. Bull Johns Hopkins Hosp 94:238–282.
Ruggero MA, Rich NC (1987) Timing of spikes initiation in cochlear afferents: dependence on site of innervation. J Neurophysiol 58:379–403.
Ruggero MA, Rich NC, Recio A, Narayan SS, Robles L (1997) Basilar-membrane responses to tones at the base of the chinchilla cochlea. J Acoust Soc Am 101:2151–2163.
Sawtell NB, Williams A, Roberts PD, von der Emde G, Bell CC (2006) Effects of sensing behavior on a latency code. J Neurosci 26:8221–8234.
Shera CA, Talmadge CL, Tubis A (2000) Interrelations among distortion-product phase-gradient delays: their connection to scaling symmetry and its breaking. J Acoust Soc Am 108:2933–2948.
Shusterman R, Smear MC, Koulakov AA, Rinberg D (2011) Precise olfactory responses tile the sniff cycle. Nat Neurosci 14:1039–1044.
Smith RL, Brachman ML (1980) Response modulation of auditory-nerve fibers by AM stimuli: effects of average intensity. Hear Res 2:123–133.
Stern RM, Zeiberg AS, Trahiotis C (1988) Lateralization of complex binaural stimuli: a weighted-image model. J Acoust Soc Am 84:156–165.
Temchin AN, Ruggero MA (2010) Phase-locked responses to tones of chinchilla auditory nerve fibers: implications for apical cochlear mechanics. J Assoc Res Otolaryngol 11:297–318.
Tollin DJ, Koka K (2009) Postnatal development of sound pressure transformations by the head and pinnae of the cat: binaural characteristics. J Acoust Soc Am 126:3125–3136.
Tollin DJ, Yin TC (2005) Interaural phase and level difference sensitivity in low-frequency neurons in the lateral superior olive. J Neurosci 25:10648–10657.
van der Heijden M, Joris PX (2003) Cochlear phase and amplitude retrieved from the auditory nerve at arbitrary frequencies. J Neurosci 23:9194–9198.
van der Heijden M, Joris PX (2006) Effects of stimulus intensity on phase and amplitude characteristics of auditory nerve fibers. Assoc Res Otolaryngol Abs 29:28–29.
VanRullen R, Guyonneau R, Thorpe SJ (2005) Spike times make sense. Trends Neurosci 28:1–4.
Versteegh CP, Meenderink SW, van der Heijden M (2011) Response characteristics in the apex of the gerbil cochlea studied through auditory nerve recordings. J Assoc Res Otolaryngol 12:301–316.
Viete S, Pena JL, Konishi M (1997) Effects of interaural intensity difference on the processing of interaural time difference in the owl's nucleus laminaris. J Neurosci 17:1815–1824.
Wightman FL, Kistler DJ (1992) The dominant role of low-frequency interaural time differences in sound localization. J Acoust Soc Am 91:1648–1661.
Yin TC, Chan JC (1990) Interaural time sensitivity in medial superior olive of cat. J Neurophysiol 64:465–488.
Yin TC, Kuwada S (1983a) Binaural interaction in low-frequency neurons in inferior colliculus of the cat. II. Effects of changing rate and direction of interaural phase. J Neurophysiol 50:1000–1019.
Yin TC, Kuwada S (1983b) Binaural interaction in low-frequency neurons in inferior colliculus of the cat. III. Effects of changing frequency. J Neurophysiol 50:1020–1042.
Yin TC, Hirsch JA, Chan JC (1985) Responses of neurons in the cat's superior colliculus to acoustic stimuli. II. A model of interaural intensity sensitivity. J Neurophysiol 53:746–758.
Zohar O, Shackleton TM, Nelken I, Palmer AR, Shamir M (2011) First spike latency code for interaural phase difference discrimination in the guinea pig inferior colliculus. J Neurosci 31:9192–9204.